

Realization of Isolated and High-Density Skyrmions at Room Temperature in Uncompensated Synthetic Antiferromagnets

Ruyi Chen,[▽] Yang Gao,[▽] Xichao Zhang, Ruiqi Zhang, Siqi Yin, Xianzhe Chen, Xiaofeng Zhou, Yongjian Zhou, Jing Xia, Yan Zhou, Shouguo Wang, Feng Pan, Ying Zhang,* and Cheng Song*

Cite This: *Nano Lett.* 2020, 20, 3299–3305

Read Online

ACCESS |

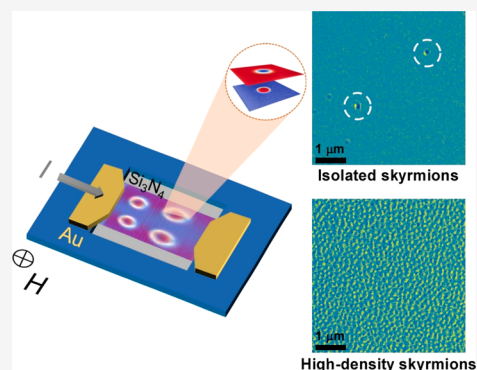
Metrics & More

Article Recommendations

Supporting Information

ABSTRACT: Magnetic skyrmions are vortex-like spin textures with nontrivial spin topology and novel physical properties that show promise as an essential building block for novel spintronic applications. Skyrmions in synthetic antiferromagnets (SAF) have been proposed long-term to have many advantages than those in ferromagnetic materials, which suffer from fundamental limits for size and efficient manipulation. Thus, experimental realization of skyrmions in SAF is intensely pursued. Here we show the observation of zero-field stable magnetic skyrmions at room temperature in SAF [Co/Pd]/Ru/[Co/Pd] multilayers with Lorentz transmission electron microscope, where uncompensated moments of the SAF provide a medium for the skyrmion characterization. Isolated skyrmions and high-density skyrmions via magnetic field and electromagnetic coordinated methods have been observed, respectively. These created high-density skyrmions maintain at zero-field even when both the current and magnetic field are removed. The use of skyrmions in SAF would advance the process toward practical nonvolatile memories based on spin topology.

KEYWORDS: skyrmion, synthetic antiferromagnet, electromagnetic coordinated method, Ruderman–Kittel–Kasuya–Yosida interaction



Magnetic skyrmions are a topological field configuration that exhibit fascinating physical behaviors^{1–5} and have been an important theme of condensed matter physics for many years.^{6–9} The magnetic skyrmion was experimentally detected in 2009³ in bulk ferromagnetic materials with Dzyaloshinskii–Moriya interaction (DMI). Subsequently, skyrmions were also proved to exist in ultrathin magnetic multilayers.^{2,4,10–14} In fact, magnetic skyrmions in thin films are notably interesting where the spin–orbit coupling (SOC) and magnetic interactions are able expediently engineered by the thickness of layer,¹¹ relative components,¹³ and repetition periods.¹⁴ Moreover, the interfacial DMI from symmetry-breaking systems and the strong SOC from heavy metals develop a preferred chirality for spin textures, which makes it possible to stabilize skyrmions and reduce the skyrmion size at the same time.^{1,13,15,16} Furthermore, their stiffness derived from the topological properties and their particle-like properties make them promising for information technologies.^{15,17,18}

Recent progress in nanotechnology has demonstrated that topological spin textures in ferromagnetic system are sensitive to different external excitations, such as magnetic field,^{4,5,12} electric current/field,^{19–23} and thermal gradient.^{23–25} Complex electromagnetic dynamics can be observed under the interaction of these external excitations with noncollinear magnetic spin structures. However, skyrmions in ferromagnets are basically limited by the stray magnetic field interaction limiting bit size²⁶

and precessional dynamics limiting the operation speed,^{27,28} which hinders further development. Especially, skyrmion Hall effect (SkHE)^{6,29,30} is a major obstacle that restricts the essential transmission of skyrmions in the device, where skyrmions feel the Magnus force, causing the movement trajectory of the skyrmions to deviate from the driving current direction. As a result, the skyrmions carrying encoded information may be destroyed at the edge of the racetrack, which may lead to the annihilation of the skyrmions and loss of stored information. This will be a roadblock to the realization of spintronic devices which make use of magnetic skyrmions as information carriers.³¹ However, antiferromagnets (AFMs) with zero net magnetic moment are foreseen to be an extraordinary system for skyrmions^{32–35} for the absence of stray field and skyrmion Hall effect. Several methods have been proposed,^{32,36,37} however, it is still difficult to experimentally manipulate and detect antiferromagnetic spin textures. More recently, skyrmions were obtained in ferrimagnetic materials, which exhibit the advantages of antiferromagnetically exchange-coupled sky-

Received: January 10, 2020

Revised: April 2, 2020

Published: April 13, 2020



rmions.^{38,39} Nevertheless, skyrmions in ferrimagnetic materials are sensitive to temperature disturbance, which is unfavorable for spintronic applications.

SAF based on the Ruderman–Kittel–Kasuya–Yosida (RKKY) coupling,^{40,41} where the bottom and top ferromagnets are coupled through the antiferromagnetic exchange interaction, has the advantages of high stability and zero stray field analogous to those in AFMs, whereas they stay easy to detect and manipulate with external stimuli. Most recently, we found two pioneering works reporting that skyrmions/skyrmion bubbles are observed in synthetic AFMs using magnetic force microscopy⁴² and magneto-optical polar Kerr effect microscopy.⁴³ The authors utilize interlayer coupling to a neighbor bias layer, and isolated antiferromagnetic skyrmions can be stabilized.⁴² The other work achieved the formation and movement of skyrmion bubbles in SAF via engineering the multilayers to make use of DMI and spin–orbit torque.⁴³ Here, we show how the simple electromagnetic coordinated method⁴⁴ works on the antiparallel aligned spin structures to generate high-density skyrmions instead of isolated skyrmions at room temperature in uncompensated SAF structures, which is significant to realize the conception of skyrmion-based spintronic applications.

Stack films of Pt(2.5)/[Co(0.43)/Pd(0.8)]₁₂/Ru(0.6)/[Co(0.43)/Pd(0.8)]₆/Pd(2) (sample F1) and Ta(4)/Pt(6)/[Co(0.43)/Pd(0.8)]₉/Ru(0.6)/[Co(0.43)/Pd(0.8)]₉/Pd(2) (sample F2) ([Co/Pd]/Ru/[Co/Pd] for short, units in nanometer) were deposited on Si₃N₄ membrane windows via magnetron sputtering (see Methods), as illustrated in Figure 1a,b. In order to achieve antiferromagnetic coupling for the top and bottom ferromagnetic layers, the thickness of Ru is designed to be 0.6 nm. Ta/Pt buffer layer is deposited to obtain a stronger perpendicular magnetic anisotropy (PMA) of Co-based multilayers in F2 which is designed as a control sample. Figure 1c,d presents the hysteresis loops of samples F1 and F2, respectively. In Figure 1c, obvious antiferromagnetic coupling is observed where the moments begin to reverse at a positive field in the descending branch, in contrast to magnetization reversal at a negative field for sample F2 (Figure 1d), which is difficult to identify the antiferromagnetic coupling. To confirm this, a minor loop of F2 is measured (see Figure S1, Supporting Information). The positive shift in that minor loop is suggestive of the antiferromagnetic coupling between the top and bottom Co/Pd multilayers. The most striking feature for these two curves is the sharp switching reversal edges of the magnetization curve of F2, in contrast to a sluggish reversal feature for F1, indicating a stronger PMA of F2 as we designed. It is worth noting that the kink near zero field in hysteresis loops corresponds to the reversal of Pd, because the magnetic moment in the Pd layer cannot be ignored due to the hybridization of d-shell electrons at the Co/Pd interface.⁴⁵

We now focus on the skyrmion evolution modulated by the electromagnetic coordinated method in our SAF samples. Figure 2 shows the simulated magnetic structure and concomitant Lorentz transmission electron microscope (L-TEM) images of magnetic domains in sample F1 at room temperature. For these experiments, the observation of magnetic domains was realized through the L-TEM under different external magnetic fields ($\mu_0 H$) along the beam propagation direction (denoted as the $-z$ direction; Figure 1e) by raising the objective lens current step by step. The manipulation of skyrmion behavior via current was performed by using a TEM holder where both sides of the TEM sample had electrical

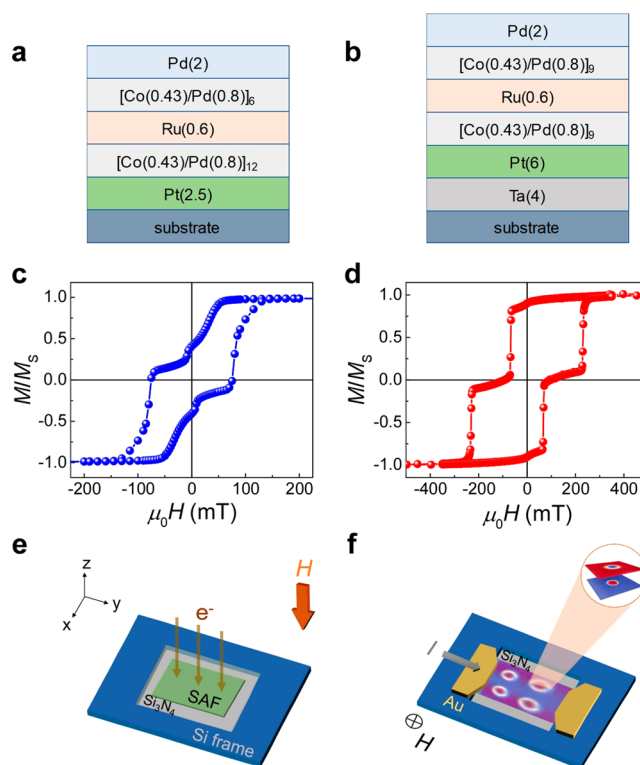


Figure 1. Sample geometry and magnetic properties of SAF with different stacking modes. (a,b) Schematic configuration of SAF with weak PMA (a) and strong PMA (b). The numbers in parentheses are the thickness in nanometers. (c,d) Corresponding out-of-plane hysteresis loops of the films. Experimental geometry for L-TEM imaging where only the magnetic field (e) and electromagnetic coordinated method were carried out (f), respectively. The Si₃N₄ window is 0.1 mm \times 0.1 mm and 20 nm thick.

conducting blocks, as shown in Figure 1f. L-TEM images were obtained with a negative defocus and a tilting angle of -15° along the x -axis. Figure 2a presents the simulated spin structures in SAF, where the top and bottom [Co/Pd] layers exhibit a parallel-aligned uniform state. The L-TEM image at $\mu_0 H = 145$ mT is shown in Figure 2e. The uniform domain indicates the upward alignment of moments corresponding to the saturated state in Figure 2a. By gradually decreasing the magnetic field to a low field of 18 mT, two isolated skyrmions with the diameter of ~ 80 nm are obtained in $5 \mu\text{m} \times 5 \mu\text{m}$ scale, as displayed in Figure 2f. Their spin structure can be described by the head-to-head “ $\downarrow\uparrow$ ” (the center of skyrmions) and tail-to-tail “ $\uparrow\downarrow$ ” (the edge of skyrmions) antiparallel states for the top and bottom [Co/Pd] layers, as illustrated in Figure 2b. Three typical L-TEM images recorded at -15° , 0° , and 15° exhibit the reversal contrast (see Figure S2, Supporting Information), indicating that the skyrmions stabilized at room temperature are Néel-type skyrmions.⁴⁶

We then discuss the generation of high-density skyrmions. Current pulses with a current density of 1.1×10^9 A/m² were applied to the uniform SAF sample F1 using the experimental schematic displayed in Figure 1f. It is found that typical labyrinth domains emerge as presented in Figure 2g, where the top and bottom [Co/Pd] layers show a spiral state (Figure 2c). Note that the spiral stripe created by the current may be ascribed to the spin–orbit torques and heating effects.^{44,47} Furthermore, electromagnetic coordinated manipulation was performed via applying the current pulse under a constant perpendicular $\mu_0 H$

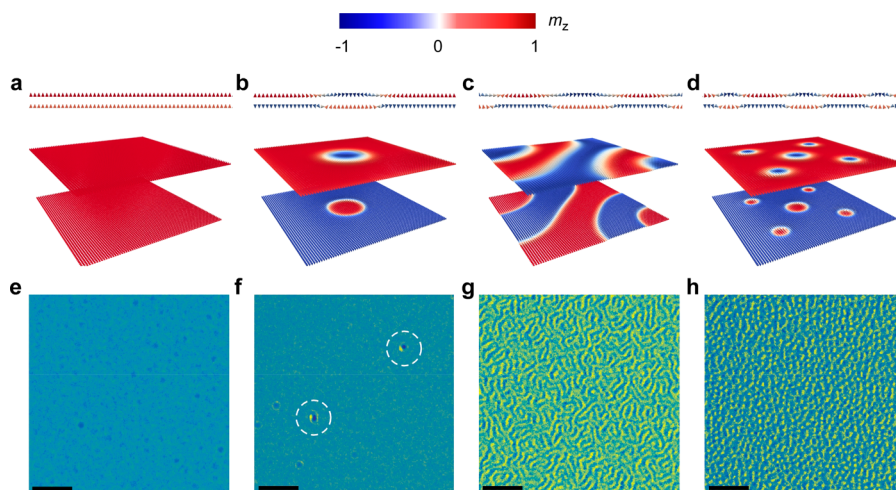


Figure 2. Simulated magnetic structure and L-TEM images of magnetic textures in SAF at room temperature. (a–d) Side view (top panels) and oblique view (bottom panels) of spin structures in sample F1, where the top and bottom [Co/Pd] layers show a parallel-aligned uniform state (a), isolated skyrmion state with antiparallel-aligned spin structure (b), spiral state (c), and high-density skyrmions state with antiparallel-aligned spin structure (d). Note that the side view is given along the diagonal. (e–h) Under-focused L-TEM images of F1 SAF at 145 mT (e), at 18 mT after being saturated (f), at zero field after applying current pulse (g) and after applying current pulse at 40 mT (h), corresponding to the magnetic structures shown in (a–d), respectively. Isolated skyrmions are highlighted by circles in (f) for clarity. The scale bar in L-TEM images corresponds to 1 μm . The cones in simulated structures represent the directions of spin. The perpendicular component of spin (m_z) is color-coded (spins point along +z, -z, and in-plane are denoted by red, blue, and white, respectively).

of 40 mT. The labyrinth domains transform into high-density skyrmions with approximately 900 skyrmions in a 5 $\mu\text{m} \times 5 \mu\text{m}$ scale. It is noteworthy that the created high-density skyrmions sustain even after the external magnetic field and electric current are removed, as shown in Figure 2h. The spin structure for each skyrmion is supposed to be similar to the isolated counterpart, as displayed in Figure 2d. Interestingly, the created high-density skyrmions via the electromagnetic manipulation are confirmed to be robust after several days in the field-free and vacuum environment at room temperature. However, due to the large pinning effect in Co/Pd multilayers, we cannot observe the current-driven motion of these skyrmions. The nonvolatile high-density skyrmion is implemented in the SAF multilayer structure without any external field support and no geometric constraint, making it a promising candidate for future nonvolatile memory device applications.

The situation differs dramatically for sample F2, which is also a SAF [Co/Pd]/Ru/[Co/Pd] but with a stronger PMA. An identical experimental procedure, including the electromagnetic manipulation method, was performed on F2, whereas there is no skyrmion observed in this sample (see Figure S1, Supporting Information). In our multilayer samples, strong interfacial SOC in the multilayer leads to an interfacial DMI. The interface DMI acts as an in-plane effective field that breaks the symmetry, which can stabilize Néel-type domain walls with a preferred chirality and resultant skyrmions.⁴⁸ However, a strong PMA in the system results in the uniform magnetization at the ground state of the bottom and top ferromagnets that is unfavorable to form a noncollinear order, which can explain the absence of skyrmions in sample F2.

To further comprehend the effect of the various magnetic parameters on the skyrmion characteristics in SAF, we carry out micromagnetic simulations for the SAF skyrmions and study how the skyrmions evolution is affected by DMI, PMA, and interlayer exchange interaction strength at zero-field (see Section S3, Supporting Information). Considering that the skyrmions in SAF are composed of two components (top and

bottom ferromagnetic layers) with antiferromagnetic coupling, we could select one of the layers to investigate the spin structure of SAF skyrmions. Figure 3a illustrates the simulated diameter of

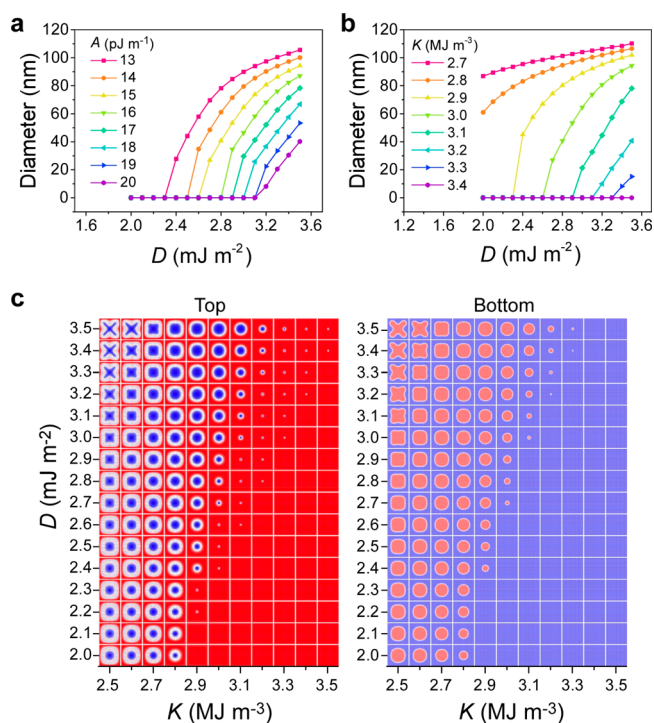


Figure 3. Simulated diameter of zero-field skyrmion and skyrmion phase diagram in SAF. (a,b) DMI constant D dependent skyrmion diameter for different interlayer exchange constant A (a) and PMA constant K (b). (c) Skyrmion phase diagram of [Co/Pd]/Ru/[Co/Pd] SAF as a function of DMI constant D and PMA constant K for both bottom and top ferromagnetic layers. The out-of-plane component of spin (m_z) points along +z, -z, and in-plane are denoted by red, blue, and white, respectively.

skyrmions in the bottom [Co/Pd] layer of the SAF as a function of the values of DMI constant D in the range of $2.0\text{--}3.5\text{ mJ m}^{-2}$ for different interlayer exchange interaction constant A in the range of $13\text{--}20\text{ pJ m}^{-1}$. Remarkably, the skyrmion diameter increases with increasing D , whereas it decreases with increasing A . Also visible is that a larger D is necessary to stabilize skyrmions for the enhanced A . The DMI constant D dependent skyrmion diameter in the bottom layer of the SAF for different PMA constant K is presented in Figure 3b, where D and K are in the range $2.0\text{--}3.5\text{ mJ m}^{-2}$ and $2.7\text{--}3.4\text{ MJ m}^{-3}$, respectively. Remarkably, the skyrmion diameter is reduced for increasing K . It is also found that the diameter stays zero for all of the selected D when the anisotropy K is up to 3.4 MJ m^{-3} , reflecting that the skyrmion cannot be formed with a large PMA, which agrees well with the case of sample F2 possessing a very strong PMA. The phenomena above can be understood that a stronger PMA and strong interlayer exchange interaction A in the multilayers is unfavorable to form a noncollinear order. Differently, the interfacial DMI works as an in-plane effective field that breaks the symmetry, which favors the rotation of skyrmion magnetization and its expansion.⁴⁹

We display in the left panel of Figure 3c the skyrmion phase diagram of [Co/Pd]/Ru/[Co/Pd] SAF as a function of DMI constant D and PMA constant K . Concerning the top [Co/Pd] layer of the SAF, the size of skyrmions increases with increasing D , whereas it is reduced with increasing K . Also visible is that the size of the skyrmions is reduced with increasing K for a certain D , accompanied by the absence of skyrmions with a large K and small D . The absence of skyrmions here is consistent with our experimental results that the sample F2 with strong PMA cannot possess a skyrmion state via the electromagnetic manipulation method. A detailed inspection shows the formation of spiral states rather than skyrmions with enhancing D for a rather small K of 2.5 MJ m^{-3} . Similar results are obtained for the bottom [Co/Pd] layers in the right panel of Figure 3c, because the top and bottom components of the skyrmions always exhibit antiferromagnetic coupling. The interlayer exchange interaction constant A dependent skyrmion phase diagram shows that the size of skyrmions increases with increasing D , whereas it is reduced with increasing A (see Figure S3, Supporting Information). In addition, we performed the simulations on a skyrmion diagram as functions of applied magnetic field and magnetic parameters where the magnetization states (i.e., the uniform state, isolated skyrmions state, spiral state, and high-density skyrmions state) and skyrmions size vary with the external magnetic field and magnetic parameters (see Note 5, Supporting Information). The current-induced motion of isolated skyrmions in the SAF with different compensation ratio was simulated, and the elimination of skyrmion Hall effect was obtained at the compensated SAF (see Figure S10, Supporting Information). There is no lateral shift observed at this scenario, which is supported by the videos showing the skyrmion motion at selected compensation ratio n and damping constant α (see Movies S1–S3).

We finally discuss whether the electromagnetic manipulation method is effective for the generation of skyrmions in other SAF structures. A sample with three [Co/Pd] multilayers separated by two 0.6 nm-thick Ru layers is designed to investigate the skyrmions, where the antiferromagnetic coupling is introduced via the Ru spacer, as displayed in Figure 4a. Figure 4b exhibits hysteresis loops of the [Co/Pd]/Ru/[Co/Pd]/Ru/[Co/Pd] structure at room temperature. Two antiferromagnetic plateaus can be observed, reflecting the antiferromagnetic coupling

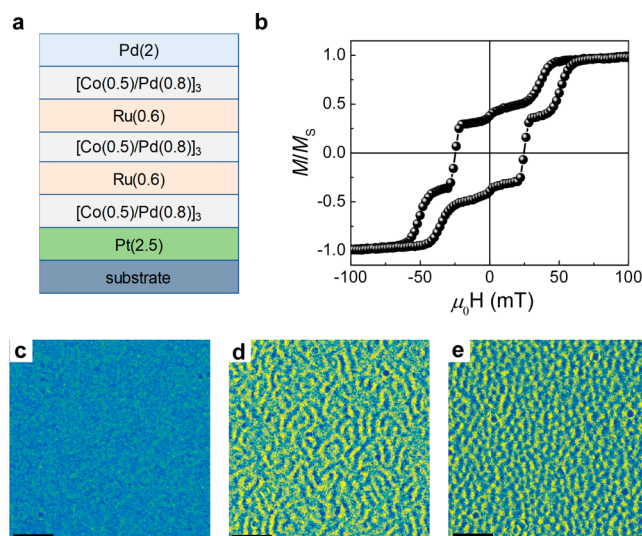


Figure 4. Stabilization of skyrmions in [Co/Pd]/Ru/[Co/Pd]/Ru/[Co/Pd] SAF with three ferromagnetic layers at room temperature. (a) Schematic of the SAF sample design with three ferromagnetic layers. (b) Out-of-plane hysteresis loops of the stack shown in (a). (c–e) L-TEM images of the SAF recorded at $\mu_0H = 0$ without current pulse (c), after applying the current pulses at $\mu_0H = 0$ (d) and after applying the current pulses at $\mu_0H = 40\text{ mT}$ (e). The scale bar in L-TEM images corresponds to $1\ \mu\text{m}$.

feature. Also, the hysteresis loops behave as slanted magnetization switching, revealing the existence of weak PMA. Figure 4c–e presents L-TEM pictures of the SAF recorded at $\mu_0H = 0$ without a current pulse, after applying the current pulses with a current density of $2.0 \times 10^9\text{ A/m}^2$ at $\mu_0H = 0$ and after applying the current pulses at $\mu_0H = 40\text{ mT}$, respectively. It appears in Figure 4c that the film without any external stimulus shows a uniform state. Clearly, labyrinth domains emerge as the current pulses are applied (Figure 4d), and high-density skyrmions are created after applying the magnetic field and current pulse simultaneously (Figure 4e). Such high-density skyrmions show a density approximately of 700 in $5\ \mu\text{m} \times 5\ \mu\text{m}$ scale, which are quite stable in a field-free environment at room temperature. Thus, the created field-free high-density skyrmions by the electromagnetic coordinated method are reliable even in SAF with three ferromagnetic layers. On the other hand, isolated skyrmions are also observed in the SAF structure with three ferromagnetic layers, and the corresponding L-TEM image is recorded (see Figure S11, Supporting Information). This method is expected to be generalized to other complex SAF systems which may be necessary for the functional devices based on skyrmions.

In summary, both isolated and high-density skyrmions at room temperature are observed in uncompensated uniform SAF by L-TEM. The diameter of the skyrmions is approximately 80 nm, while the density of the observed skyrmions is up to 900 in $5\ \mu\text{m} \times 5\ \mu\text{m}$ scale. Isolated skyrmions can be obtained after saturating the films at a large external magnetic field and then decreasing the field to 18 mT. High-density skyrmions are created through applying a combination of electric current and magnetic field, that is, electromagnetic coordinated methods. Both the experiments and micromagnetic simulation disclose that the skyrmions cannot be formed in SAF with a strong PMA. Micromagnetic modeling of skyrmions in SAF shows that the size of skyrmions increases with increasing DMI constant D , but shrinks with enhancing interlayer exchange interaction constant

A and PMA constant K . All of the created high-density skyrmions are quite robust in the field-free experiments at room temperature, which is a significant step in terms of designing functional devices based on magnetic skyrmions. Our experimental finding adds a novel dimension to create skyrmions in synthetic AFMs and would advance the development of skyrmion-based logic and memory devices.

METHODS

Thin-Film Growth and Imaging. The films were deposited at room temperature on a 20 nm-thick Si_3N_4 membrane window for L-TEM observation and the thermally oxidized Si/SiO₂ substrates for magnetic property measurements via dc magnetron sputtering with a base vacuum better than 8.0×10^{-5} mTorr, and the working argon pressure was 3 mTorr. The magnetization measurements were carried via a superconducting quantum interference device magnetometer at room temperature. The domain images were obtained via a L-TEM (JEOL 2100F) under external magnetic fields by raising the objective lens current step-by-step. The manipulation of skyrmion behavior via current was performed by using a TEM holder where both sides of the TEM sample have electrical conducting blocks. Current pulses used during the electric manipulation are the typical square wave with 150 μs pulse width for total 100 points. A source-measure unit instrument (Keithley 2601B) was supplied as the dc current.

ASSOCIATED CONTENT

Supporting Information

The Supporting Information is available free of charge at <https://pubs.acs.org/doi/10.1021/acs.nanolett.0c00116>.

Comparative experiments on the skyrmions characterization for F2 synthetic antiferromagnetic sample; experimental L-TEM images of a Néel skyrmion at different tilt angles; image simulation and micromagnetic modeling; interlayer exchange interaction dependent skyrmion phase diagram in SAF; simulations on skyrmion diagram as functions of applied magnetic field and magnetic parameters in SAF; simulations on the current-induced movement of isolated skyrmions in SAF (PDF)

Movie S1: Motion of isolated skyrmion induced by current in SAF at the compensation ratio $n = 0.90$ and damping constant $\alpha = 0.3$ (MP4)

Movie S2: Motion of isolated skyrmion induced by current in SAF at the compensation ratio $n = 1.00$ and damping constant $\alpha = 0.3$ (MP4)

Movie S3: Motion of isolated skyrmion induced by current in SAF at the compensation ratio $n = 1.02$ and damping constant $\alpha = 0.3$ (MP4)

AUTHOR INFORMATION

Corresponding Authors

Ying Zhang – Beijing National Laboratory for Condensed Matter Physics, Institute of Physics, Chinese Academy of Sciences, Beijing 100190, China; Songshan Lake Materials Laboratory, Dongguan, Guangdong 523808, China; orcid.org/0000-0001-5476-1524; Email: zhangy@iphy.ac.cn

Cheng Song – Key Laboratory of Advanced Materials (MOE), School of Materials Science and Engineering, Tsinghua University, Beijing 100084, China; orcid.org/0000-0002-7651-9031; Email: songcheng@mail.tsinghua.edu

Authors

Ruyi Chen – Key Laboratory of Advanced Materials (MOE), School of Materials Science and Engineering, Tsinghua University, Beijing 100084, China

Yang Gao – Beijing National Laboratory for Condensed Matter Physics, Institute of Physics, Chinese Academy of Sciences, Beijing 100190, China; Institute of Advanced Materials, Beijing Normal University, Beijing 100875, China

Xichao Zhang – School of Science and Engineering, The Chinese University of Hong Kong, Shenzhen, Guangdong 518172, China

Ruiqi Zhang – Key Laboratory of Advanced Materials (MOE), School of Materials Science and Engineering, Tsinghua University, Beijing 100084, China

Siqi Yin – Key Laboratory of Advanced Materials (MOE), School of Materials Science and Engineering, Tsinghua University, Beijing 100084, China

Xianzhe Chen – Key Laboratory of Advanced Materials (MOE), School of Materials Science and Engineering, Tsinghua University, Beijing 100084, China

Xiaofeng Zhou – Key Laboratory of Advanced Materials (MOE), School of Materials Science and Engineering, Tsinghua University, Beijing 100084, China

Yongjian Zhou – Key Laboratory of Advanced Materials (MOE), School of Materials Science and Engineering, Tsinghua University, Beijing 100084, China

Jing Xia – School of Science and Engineering, The Chinese University of Hong Kong, Shenzhen, Guangdong 518172, China

Yan Zhou – School of Science and Engineering, The Chinese University of Hong Kong, Shenzhen, Guangdong 518172, China

Shouguo Wang – Institute of Advanced Materials, Beijing Normal University, Beijing 100875, China

Feng Pan – Key Laboratory of Advanced Materials (MOE), School of Materials Science and Engineering, Tsinghua University, Beijing 100084, China

Complete contact information is available at:

<https://pubs.acs.org/doi/10.1021/acs.nanolett.0c00116>

Author Contributions

[▽]These authors contributed equally. C.S. and R.C. designed the experiment. Y.Z. and Y.G. carried out the L-TEM measurements. Y.Z., X.Z., and J.X. performed the micromagnetic simulation. C.S., R.C., and X.Z. wrote the paper. All authors discussed results and reviewed the manuscript.

Notes

The authors declare no competing financial interest.

ACKNOWLEDGMENTS

C.S. acknowledges the support of the Beijing Innovation Center for Future Chips, Tsinghua University and the Young Chang Jiang Scholars Programme. This work was supported by the National Key R&D Programme of China (grant no. 2017YFB0405704), the National Natural Science Foundation of China (grant nos. 51871130, 11874408, and 51671110), Fujian Institute of Innovation, Chinese Academy of Sciences (grant no. FJCX18040302), and Youth Innovation Promotion Association, CAS, 2015004. X.Z. was supported by the Guangdong Basic and Applied Basic Research Foundation (Grant No. 2019A1515110713), and the Presidential Postdoctoral Fellowship of The Chinese University of Hong Kong, Shenzhen (CUHKSZ). Y.Z. acknowledges the support by the President's Fund of CUHKSZ, Longgang Key Laboratory of Applied Spintronics, National Natural Science Foundation of

China (grant nos. 11974298 and 61961136006), Shenzhen Fundamental Research Fund (grant no. JCYJ20170410171958839), and Shenzhen Peacock Group Plan (grant no. KQTD20180413181702403).

REFERENCES

- (1) Rossler, U. K.; Bogdanov, A. N.; Pflleiderer, C. Spontaneous skyrmion ground states in magnetic metals. *Nature* **2006**, *442*, 797.
- (2) Yu, X. Z.; Onose, Y.; Kanazawa, N.; Park, J. H.; Han, J. H.; Matsui, Y.; Nagaosa, N.; Tokura, Y. Real-space observation of a two-dimensional skyrmion crystal. *Nature* **2010**, *465*, 901.
- (3) Mühlbauer, S.; Binz, B.; Jonietz, F.; Pflleiderer, C.; Rosch, A.; Neubauer, A.; Georgii, R.; Böni, P. Skyrmion Lattice in a Chiral Magnet. *Science* **2009**, *323*, 915.
- (4) Heinze, S.; von Bergmann, K.; Menzel, M.; Brede, J.; Kubetzka, A.; Wiesendanger, R.; Bihlmayer, G.; Blügel, S. Spontaneous atomic-scale magnetic skyrmion lattice in two dimensions. *Nat. Phys.* **2011**, *7*, 713.
- (5) Yu, X. Z.; Kanazawa, N.; Onose, Y.; Kimoto, K.; Zhang, W. Z.; Ishiwata, S.; Matsui, Y.; Tokura, Y. Near room-temperature formation of a skyrmion crystal in thin-films of the helimagnet FeGe. *Nat. Mater.* **2011**, *10*, 106.
- (6) Nagaosa, N.; Tokura, Y. Topological properties and dynamics of magnetic skyrmions. *Nat. Nanotechnol.* **2013**, *8*, 899.
- (7) Zhang, X.; Zhou, Y.; Song, K. M.; Park, T. E.; Xia, J.; Ezawa, M.; Liu, X.; Zhao, W.; Zhao, G. P.; Woo, S. Skyrmion-electronics: Writing, deleting, reading and processing magnetic skyrmions toward spintronic applications. *J. Phys.: Condens. Matter* **2020**, *32*, 143001.
- (8) Wiesendanger, R. Nanoscale magnetic skyrmions in metallic films and multilayers: a new twist for spintronics. *Nat. Rev. Mater.* **2016**, *1*, 16044.
- (9) Fert, A.; Reyren, N.; Cros, V. Magnetic skyrmions: advances in physics and potential applications. *Nat. Rev. Mater.* **2017**, *2*, 17031.
- (10) Dupe, B.; Hoffmann, M.; Paillard, C.; Heinze, S. Tailoring magnetic skyrmions in ultra-thin transition metal films. *Nat. Commun.* **2014**, *5*, 4030.
- (11) Yu, G.; Upadhyaya, P.; Li, X.; Li, W.; Kim, S. K.; Fan, Y.; Wong, K. L.; Tserkovnyak, Y.; Amiri, P. K.; Wang, K. L. Room-Temperature Creation and Spin-Orbit Torque Manipulation of Skyrmions in Thin Films with Engineered Asymmetry. *Nano Lett.* **2016**, *16*, 1981.
- (12) Woo, S.; Litzius, K.; Kruger, B.; Im, M. Y.; Caretta, L.; Richter, K.; Mann, M.; Krone, A.; Reeve, R. M.; Weigand, M.; Agrawal, P.; Lemesh, I.; Mawass, M. A.; Fischer, P.; Klau, M.; Beach, G. S. Observation of room-temperature magnetic skyrmions and their current-driven dynamics in ultrathin metallic ferromagnets. *Nat. Mater.* **2016**, *15*, 501.
- (13) Soumyanarayanan, A.; Raju, M.; Gonzalez Oyarce, A. L.; Tan, A. K. C.; Im, M. Y.; Petrovic, A. P.; Ho, P.; Khoo, K. H.; Tran, M.; Gan, C. K.; Ernult, F.; Panagopoulos, C. Tunable room-temperature magnetic skyrmions in Ir/Fe/Co/Pt multilayers. *Nat. Mater.* **2017**, *16*, 898.
- (14) Moreau-Luchaire, C.; Moutafis, C.; Reyren, N.; Sampaio, J.; Vaz, C. A. F.; Van Horne, N.; Bouzehouane, K.; Garcia, K.; Deranlot, C.; Warnicke, P.; Wohlhuter, P.; George, J.-M.; Weigand, M.; Raabe, J.; Cros, V.; Fert, A. Additive interfacial chiral interaction in multilayers for stabilization of small individual skyrmions at room temperature. *Nat. Nanotechnol.* **2016**, *11*, 444.
- (15) Fert, A.; Cros, V.; Sampaio, J. Skyrmions on the track. *Nat. Nanotechnol.* **2013**, *8*, 152.
- (16) He, M.; Li, G.; Zhu, Z.; Zhang, Y.; Peng, L.; Li, R.; Li, J.; Wei, H.; Zhao, T.; Zhang, X.; Wang, S.; Lin, S.; Lin, G.; Yu, G.; Cai, J.; Shen, B. Evolution of topological skyrmions across the spin reorientation transition in Pt/Co/Ta multilayers. *Phys. Rev. B: Condens. Matter Mater. Phys.* **2018**, *97*, 174419.
- (17) Kiselev, N. S.; Bogdanov, A. N.; Schäfer, R.; Rößler, U. K. Chiral skyrmions in thin magnetic films: new objects for magnetic storage technologies? *J. Phys. D: Appl. Phys.* **2011**, *44*, 392001.
- (18) Parkin, S. S. P.; Hayashi, M.; Thomas, L. Magnetic Domain-Wall Racetrack Memory. *Science* **2008**, *320*, 190.
- (19) Jonietz, F.; Mühlbauer, S.; Pflleiderer, C.; Neubauer, A.; Munzer, W.; Bauer, A.; Adams, T.; Georgii, R.; Boni, P.; Duine, R. A.; et al. Spin

Transfer Torques in MnSi at Ultralow Current Densities. *Science* **2010**, *330*, 1648.

(20) Schulz, T.; Ritz, R.; Bauer, A.; Halder, M.; Wagner, M.; Franz, C.; Pflleiderer, C.; Everschor, K.; Garst, M.; Rosch, A. Emergent electrostatics of skyrmions in a chiral magnet. *Nat. Phys.* **2012**, *8*, 301.

(21) Ma, C.; Zhang, X.; Xia, J.; Ezawa, M.; Jiang, W.; Ono, T.; Piramanayagam, S. N.; Morisako, A.; Zhou, Y.; Liu, X. Electric field-induced creation and directional motion of domain walls and skyrmion bubbles. *Nano Lett.* **2019**, *19*, 353.

(22) White, J. S.; Prsa, K.; Huang, P.; Omrani, A. A.; Zivkovic, I.; Bartkowiak, M.; Berger, H.; Magrez, A.; Gavilano, J. L.; Nagy, G.; Zang, J.; Ronnow, H. M. Electric-field-induced Skyrmion distortion and giant lattice rotation in the magnetoelectric insulator Cu₂OSeO₃. *Phys. Rev. Lett.* **2014**, *113*, 107203.

(23) Lin, S. Z.; Batista, C. D.; Reichhardt, C.; Saxena, A. ac current generation in chiral magnetic insulators and Skyrmion motion induced by the spin Seebeck effect. *Phys. Rev. Lett.* **2014**, *112*, 187203.

(24) Kong, L.; Zang, J. Dynamics of an insulating Skyrmion under a temperature gradient. *Phys. Rev. Lett.* **2013**, *111*, 067203.

(25) Mochizuki, M.; Yu, X. Z.; Seki, S.; Kanazawa, N.; Koshibae, W.; Zang, J.; Mostovoy, M.; Tokura, Y.; Nagaosa, N. Thermally driven ratchet motion of a skyrmion microcrystal and topological magnon Hall effect. *Nat. Mater.* **2014**, *13*, 241.

(26) Buttner, F.; Lemesh, I.; Beach, G. S. D. Theory of isolated magnetic skyrmions: From fundamentals to room temperature applications. *Sci. Rep.* **2018**, *8*, 4464.

(27) Thiaville, A.; Rohart, S.; Jué, É.; Cros, V.; Fert, A. Dynamics of Dzyaloshinskii domain walls in ultrathin magnetic films. *Europhys. Lett.* **2012**, *100*, 57002.

(28) Martinez, E.; Emori, S.; Perez, N.; Torres, L.; Beach, G. S. D. Current-driven dynamics of Dzyaloshinskii domain walls in the presence of in-plane fields: Full micromagnetic and one-dimensional analysis. *J. Appl. Phys.* **2014**, *115*, 213909.

(29) Litzius, K.; Lemesh, I.; Krüger, B.; Bassirian, P.; Caretta, L.; Richter, K.; Büttner, F.; Sato, K.; Tretiakov, O. A.; Förster, J.; Reeve, R. M.; Weigand, M.; Bykova, I.; Stoll, H.; Schütz, G.; Beach, G. S. D.; Kläui, M. Skyrmion Hall effect revealed by direct time-resolved X-ray microscopy. *Nat. Phys.* **2017**, *13*, 170.

(30) Jiang, W.; Zhang, X.; Yu, G.; Zhang, W.; Wang, X.; Benjamin Jungfleisch, M.; Pearson, J. E.; Cheng, X.; Heinonen, O.; Wang, K. L.; Zhou, Y.; Hoffmann, A.; te Velthuis, S. G. E. Direct observation of the skyrmion Hall effect. *Nat. Phys.* **2017**, *13*, 162.

(31) Sampaio, J.; Cros, V.; Rohart, S.; Thiaville, A.; Fert, A. Nucleation, stability and current-induced motion of isolated magnetic skyrmions in nanostructures. *Nat. Nanotechnol.* **2013**, *8*, 839.

(32) Barker, J.; Tretiakov, O. A. Static and Dynamical Properties of Antiferromagnetic Skyrmions in the Presence of Applied Current and Temperature. *Phys. Rev. Lett.* **2016**, *116*, 147203.

(33) Zhang, X.; Zhou, Y.; Ezawa, M. Antiferromagnetic Skyrmion: Stability, Creation and Manipulation. *Sci. Rep.* **2016**, *6*, 24795.

(34) Zhang, X.; Ezawa, M.; Zhou, Y. Thermally stable magnetic skyrmions in multilayer synthetic antiferromagnetic racetracks. *Phys. Rev. B: Condens. Matter Mater. Phys.* **2016**, *94*, 064406.

(35) Zhang, X.; Zhou, Y.; Ezawa, M. Magnetic bilayer-skyrmions without skyrmion Hall effect. *Nat. Commun.* **2016**, *7*, 10293.

(36) Cheng, R.; Niu, Q. Dynamics of antiferromagnets driven by spin current. *Phys. Rev. B: Condens. Matter Mater. Phys.* **2014**, *89*, 081105.

(37) Hirata, Y.; Kim, D.-H.; Okuno, T.; Nishimura, T.; Kim, D.-Y.; Futakawa, Y.; Yoshikawa, H.; Tsukamoto, A.; Kim, K.-J.; Choe, S.-B.; Ono, T. Correlation between compensation temperatures of magnetization and angular momentum in GdFeCo ferrimagnets. *Phys. Rev. B: Condens. Matter Mater. Phys.* **2018**, *97*, 220403.

(38) Woo, S.; Song, K. M.; Zhang, X.; Zhou, Y.; Ezawa, M.; Liu, X.; Finizio, S.; Raabe, J.; Lee, N. J.; Kim, S. I.; Park, S. Y.; Kim, Y.; Kim, J. Y.; Lee, D.; Lee, O.; Choi, J. W.; Min, B. C.; Koo, H. C.; Chang, J. Current-driven dynamics and inhibition of the skyrmion Hall effect of ferrimagnetic skyrmions in GdFeCo films. *Nat. Commun.* **2018**, *9*, 959.

(39) Caretta, L.; Mann, M.; Buttner, F.; Ueda, K.; Pfau, B.; Gunther, C. M.; Hessing, P.; Churikova, A.; Klose, C.; Schneider, M.; Engel, D.; Marcus, C.; Bono, D.; Bagschik, K.; Eisebitt, S.; Beach, G. S. D. Fast current-driven domain walls and small skyrmions in a compensated ferrimagnet. *Nat. Nanotechnol.* **2018**, *13*, 1154.

(40) Parkin, S. S. Systematic variation of the strength and oscillation period of indirect magnetic exchange coupling through the 3d, 4d, and 5d transition metals. *Phys. Rev. Lett.* **1991**, *67*, 3598.

(41) Chen, R. Y.; Zhang, R. Q.; Liao, L. Y.; Chen, X. Z.; Zhou, Y. J.; Gu, Y. D.; Saleem, M. S.; Zhou, X. F.; Pan, F.; Song, C. Magnetic field direction dependent magnetization reversal in synthetic antiferromagnets. *Appl. Phys. Lett.* **2019**, *115*, 132403.

(42) Legrand, W.; Maccariello, D.; Ajejas, F.; Collin, S.; Vecchiola, A.; Bouzehouane, K.; Reyren, N.; Cros, V.; Fert, A. Room-temperature stabilization of antiferromagnetic skyrmions in synthetic antiferromagnets. *Nat. Mater.* **2020**, *19*, 34.

(43) Dohi, T.; DuttaGupta, S.; Fukami, S.; Ohno, H. Formation and current-induced motion of synthetic antiferromagnetic skyrmion bubbles. *Nat. Commun.* **2019**, *10*, 5153.

(44) He, M.; Peng, L.; Zhu, Z.; Li, G.; Cai, J.; Li, J.; Wei, H.; Gu, L.; Wang, S.; Zhao, T.; Shen, B.; Zhang, Y. Realization of zero-field skyrmions with high-density via electromagnetic manipulation in Pt/Co/Ta multilayers. *Appl. Phys. Lett.* **2017**, *111*, 202403.

(45) Smith, D.; Parekh, V.; E, C.; Zhang, S.; Donner, W.; Lee, T. R.; Khizroev, S.; Litvinov, D. Magnetization reversal and magnetic anisotropy in patterned Co/Pd multilayer thin films. *J. Appl. Phys.* **2008**, *103*, 023920.

(46) Pollard, S. D.; Garlow, J. A.; Yu, J.; Wang, Z.; Zhu, Y.; Yang, H. Observation of stable Néel skyrmions in cobalt/palladium multilayers with Lorentz transmission electron microscopy. *Nat. Commun.* **2017**, *8*, 14761.

(47) Lin, S.-Z. Edge instability in a chiral stripe domain under an electric current and skyrmion generation. *Phys. Rev. B: Condens. Matter Mater. Phys.* **2016**, *94*, 020402.

(48) Jiang, W.; Chen, G.; Liu, K.; Zang, J.; te Velthuis, S. G. E.; Hoffmann, A. Skyrmions in magnetic multilayers. *Phys. Rep.* **2017**, *704*, 1.

(49) Rohart, S.; Thiaville, A. Skyrmion confinement in ultrathin film nanostructures in the presence of Dzyaloshinskii-Moriya interaction. *Phys. Rev. B: Condens. Matter Mater. Phys.* **2013**, *88*, 184422.